# A NEW EFFICIENT TECHNIQUE FOR FRACTURE ANALYSIS OF STRUCTURES

by

**Kimiro Meguro* and Hatem Tagel-Din****

## ABSTRACT

A new method for fracture analysis of reinforced concrete structures is proposed. The concrete is modeled as an assembly of distinct elements made by dividing the concrete virtually. These elements are connected by distributed springs in both normal and tangential directions. The reinforcement bars are modeled as continuos springs connecting elements together. Local failure of concrete is modeled by failure of springs connecting elements when the stress calculated from forces acting on springs exceed the critical stress. The element formulation and the computer code were developed and the accuracy of the method were verified by comparing many experimental results. In these experiments, the results showed good agreement in determining the failure load, the load-deflection relations, the prediction of crack initiation, crack location and crack propagation. The formulations used to develop this method are simple and efficient in modeling the mechanical behavior of RC structures.

## INTRODUCTION

Failure analysis of reinforced concrete structures has been mainly carried out using the Finite Element Method (FEM). However, the FEM assumes that elements are connected by nodes and in most of FEM codes, these nodes are not permitted to separate during the analysis. Moreover, separation of elements at node location results in stress singularity at the crack location. The FE analysis is appropriate especially before the generation of extensive cracking. On the other hand, many techniques were developed to deal with cracks. These techniques, such as Smeared Crack approach[1], assume that no separation occurs between elements. The effects of cracking are only considered on the element stiffness matrix. Therefore, it is difficult to follow the crack propagation using smeared crack approach. This makes the prediction of the crack initiation, crack location, and crack width or length difficult. Moreover, the use of relatively large-sized elements makes this prediction of cracking properties difficult. While, Discrete Crack Methods[1] assume that the location of cracks and direction of crack propagation are predefined .

Many other methods were developed to deal with these problems. The Rigid Block and Spring Method, RBSM[2], is one of them. The main advantage of this method is that it simulates the cracking process with relatively simple technique compared with the FEM, while the main disadvantages is that crack propagation depends mainly on the element shape, size and arrangement. Spring stiffness is not calculated accurately so that the calculated displacements were not of reliable accuracy. Each element cannot behave as one body independent from surrounding elements. Thus the RBSM can be applied only to predict failure load.

One of the recent methods to deal with fracture analysis of concrete is the Modified or Extended Distinct Element Method (MDEM or EDEM)[3]. This method can follow the highly non-linear geometric changes of the structure during failure, however, the main disadvantages of this method are that in some cases accuracy is not enough for quantitative discussion and it needs relatively long CPU time compared with the FEM.

* Associate Professor, International Center for Disaster-Mitigation Engineering, Institute of Industrial Science, The University of Tokyo
** Graduate Student, Department of Civil Engineering, The University of Tokyo

The proposed method assumes that the region studied is an assembly of virtually divided small blocks. These blocks are connected by distributed springs in normal and tangential directions. The formulations for spring stiffness and spring failure conditions were developed so that the springs surrounding the element totally represent the block deformations and failure. Although simple material models and failure criteria were incorporated, the highly non-linear behavior, i.e. crack initiation and crack propagation of the studied problems could be followed with high accuracy till reaching global failure of the structure.

## ELEMENT FORMULATION

The two elements shown in Figure (1) are assumed to be connected by normal and shear springs at one contact point. In the 2-dimensional model, three degrees of freedom are considered for each element and deformations are assumed to be small. This leads to a relatively small stiffness matrix which is only of size (6X6). Stiffness matrix is developed for an arbitrary contact point with one pair of normal and shear springs as shown in Figure (1). It should be noted that the total stiffness matrix is determined by summing the stiffness matrices of individual spring around each element. Consequently, the developed stiffness matrix is an average stiffness matrix for the element according to the stress situation around the element. Failure of springs is modeled by assuming zero stiffness for the spring being considered. Equation (1) shows the upper-left quarter of stiffness matrix. In this formulation, the element stiffness matrix depends on the contact point location (distance L and the angles $\theta$ and $\alpha$) and the stiffness of normal and shear springs which are determined according to the stress and strain situations at the contact point location.

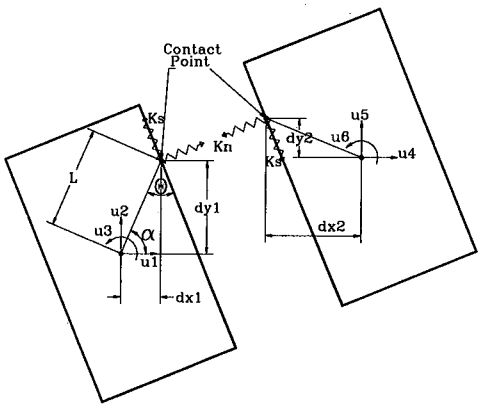


Fig. (1) Element shape, contact point and degrees of freedom for two elements

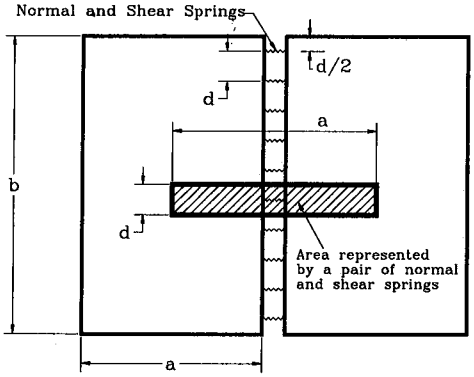


Fig. (2) Spring distributions and area of influence of each spring

$$\begin{bmatrix} \mathrm{Sin}^2(\theta+\alpha)K_n + \mathrm{Cos}^2(\theta+\alpha)K_s & -K_n\mathrm{Sin}(\theta+\alpha)\mathrm{Cos}(\theta+\alpha) + K_s\mathrm{Sin}(\theta+\alpha)\mathrm{Cos}(\theta+\alpha) & \mathrm{Cos}(\theta+\alpha)K_sL\mathrm{Sin}(\alpha) - \mathrm{Sin}(\theta+\alpha)K_nL\mathrm{Cos}(\alpha) \\ -K_n\mathrm{Sin}(\theta+\alpha)\mathrm{Cos}(\theta+\alpha) + K_s\mathrm{Sin}(\theta+\alpha)\mathrm{Cos}(\theta+\alpha) & \mathrm{Sin}^2(\theta+\alpha)K_s + \mathrm{Cos}^2(\theta+\alpha)K_n & \mathrm{Cos}(\theta+\alpha)K_nL\mathrm{Cos}(\alpha) + \mathrm{Sin}(\theta+\alpha)K_sL\mathrm{Sin}(\alpha) \\ \mathrm{Cos}(\theta+\alpha)K_sL\mathrm{Sin}(\alpha) - \mathrm{Sin}(\theta+\alpha)K_nL\mathrm{Cos}(\alpha) & \mathrm{Cos}(\theta+\alpha)K_nL\mathrm{Cos}(\alpha) + \mathrm{Sin}(\theta+\alpha)K_sL\mathrm{Sin}(\alpha) & L^2\mathrm{Cos}^2(\alpha)K_n + L^2\mathrm{Sin}^2(\alpha)K_s \end{bmatrix} \quad (1)$$

## DETERMINATION OF SPRING STIFFNESS

In this analysis, it is assumed that each normal and shear spring stiffness represents a certain area of the connected blocks. Figure (2) shows the location of springs around one edge of the element. The spring stiffness is calculated simply by Equation (2)

$$K_n = \frac{E*d*T}{a} \text{ and } K_s = \frac{G*d*T}{a} \quad (2)$$

where, d is the distance between springs, T is the thickness of the element and "a" is the length of the representative area, E and G are the Young's and shear modulus of concrete, respectively. For steel springs, the term (d*T) is replaced by the area of the steel bar while E and G are the Young's and shear modulus of steel, respectively.

## NUMERICAL ANALYSIS PROCEDURE

Figure (3) shows the flow chart of the model proposed. The program automatically generates elements and contact springs. Moreover, the reinforcement spring location is defined by its coordinate according to the position of steel bar. The global failure is achieved by having singularity in the global stiffness matrix. This singularity means that the structure has no further resistance for carrying loads. It should be noted also that using tangent modulus for the compression springs requires the use of relatively small load increments to get stable solutions. In addition, small load increments are required to follow cracking in the studied problem.

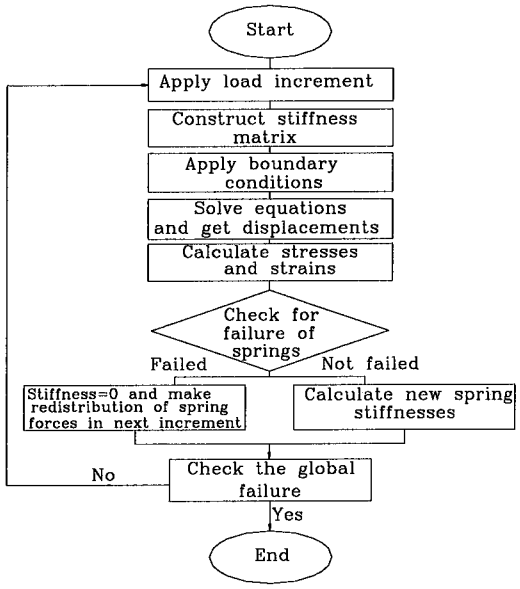


Fig. (3) Flow of analysis

## MATERIAL MODELING

Material models used for concrete are shown in Figure (4). For the tension model, Young's modulus is assumed constant till failure of springs occurs (Figure (4-a)). For the compression model, a parabolic stress-strain relation is adopted (Figure (4-b)). After reaching the peak stress, the Young's modulus is assumed to be zero to avoid negative stiffness. For the shear model, shear modulus is assumed constant till reaching the cracking point. After cracking, the shear stiffness is assumed to be zero at the location of failed springs in tension (Figure (4-c)).

As for steel, the tension and compression models are assumed to be bilinear. When steel stress reaches yield stress, Young's modulus is assumed to be 1% of its original value. After the assemblage of the global stiffness matrix, the displacements of the elements are determined using the following well-known formula

$$[K_G][U] = [F] \quad (3)$$

Where $[K_G]$ is the global stiffness matrix, [U] is the unknown displacement vector and [F] is the global load vector. After the determination of displacements, the strains are calculated by determining the new relative displacement between the ends of the springs.

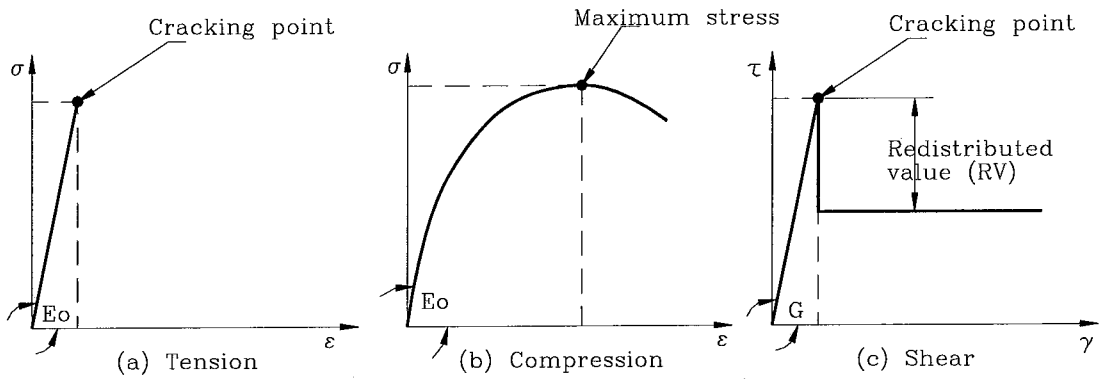

Fig. (4) Tension, compression and shear models for concrete

## FAILURE CRITERIA

One of the main problems accompanying the use of blocks for representation of reinforced concrete is the modeling of diagonal cracking. The assumption that the cracks are allowed to propagate along the element edges only increases the stiffness of the structure in nonlinear conditions. To overcome this problem, the following technique is used. It mainly depends on way of determination of the principal stresses at the contact point. Referring to Figure (5), the shear and normal stress components ($\tau$ and $\sigma_1$) at point (A) are determined from the normal and shear springs attached at the contact point location. The secondary stress ($\sigma_2$) was calculated from normal stresses in points (B) and (C), as shown in Figure (5). Therefore,

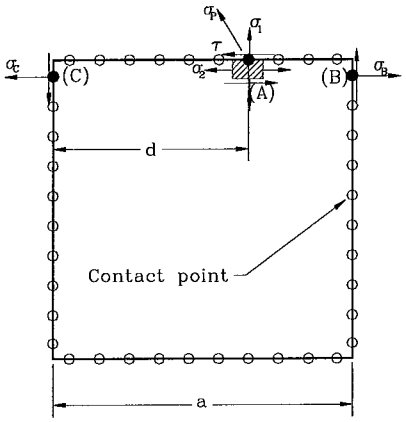

Fig. (5) Principal stress determination at contact points

$$\sigma_2 = \frac{d}{a}\sigma_B + \frac{(a-d)}{a}\sigma_C \qquad (4)$$

Hereafter, the principal tension is calculated:

$$\sigma_p = \left(\frac{\sigma_1+\sigma_2}{2}\right) + \sqrt{\left(\frac{\sigma_1-\sigma_2}{2}\right)^2 + (\tau)^2} \qquad (5)$$

This value of principal stress, $\sigma_p$, is compared with the tension resistance of concrete. When $\sigma_p$ exceeds the critical value of tension resistance, the normal and shear spring forces are redistributed in the next load increment by applying the shear and normal spring forces in the reverse direction. These redistributed forces are transferred to the element centroid as a force and moment, and then these redistributed forces are applied to the structure in the next load increment. The redistribution of spring forces at the crack location is very important for following the proper crack propagation. For the normal spring, the whole force value is redistributed to have zero tension stress at the crack faces. Although shear springs at the location of tension cracking might have some resistance after cracking due to the effect of friction and interlocking of aggregates at the crack faces, the shear stiffness is assumed zero after crack occurrence. Having any shear resistance at the crack face reduces the tendency of the crack to open in further load increments because of the rigid body motion of the attached elements. To consider the effect of friction and aggregate interlocking, a redistributed value (RV), shown in Figure (4-c), is adopted.

## SIMULATION OF THE EFFECTS OF ELEMENT SIZE AND THE NUMBER OF SPRINGS

Adjustment of element size in the analysis is very important. Simulation of structures using elements of large size leads to increasing the structure stiffness and failure resistance of the structure. This means that the calculated displacements become smaller and the failure load gets to be larger than the actual one. To make this effect clear, we carried out a series of simulations using the laterally loaded cantilever shown in Figure (6). All material properties were taken constant and elastic analysis was performed using the proposed method. The results were compared with the theoretical results of elastic structure. The percentage of error in maximum displacement and the CPU time (CPU: DEC ALPHA 300 MHz) are also shown in Figure (6). To discuss the effect of the number of connecting springs, the analyses were performed using two models with 20 and 10 springs connecting each pair of adjacent element faces for each case of different element size. From the figure, it is evident that increasing the number of base elements leads to decreasing the error but increasing the CPU time. Use of only one element at the base leads to about 30% error in the theoretically calculated displacement. This error reduces to less than 1% when the number of elements at the base increase to 5. However, the CPU time increases rapidly. When we compare the results using 20 and 10 springs, although the accuracy of the results of 10 springs model is same as that in case of 10 springs, the CPU time in case of 10 springs is almost half of that in case of 20 springs. It should be emphasized that using rigid elements, calculated displacements become smaller than the actual displacements when the size of element is not small enough. From this figure, it can be concluded that usage of large number of elements together with relatively few number of connecting springs leads to very high accuracy in reasonable analysis time. To improve the accuracy in case of elastic analysis, it is advisable to increase the number of elements rather than increasing the number of connecting springs.

It should be also noted that in the previous analysis using rigid elements, like RBSM[2], the results obtained were of poor accuracy. This may be due to:

- The spring stiffness not being determined in a proper way to simulate the element deformation,
- The use of relatively large sized elements, and
- The use of relatively small number of springs between edges which leads to an inaccurate failure mechanism.

The number of springs per face is also an important parameter. Although the effect of number of springs in the elastic analysis is not large, its effect in non-linear analysis, especially after the generation of cracks, becomes larger. This effect will be discussed in next section.

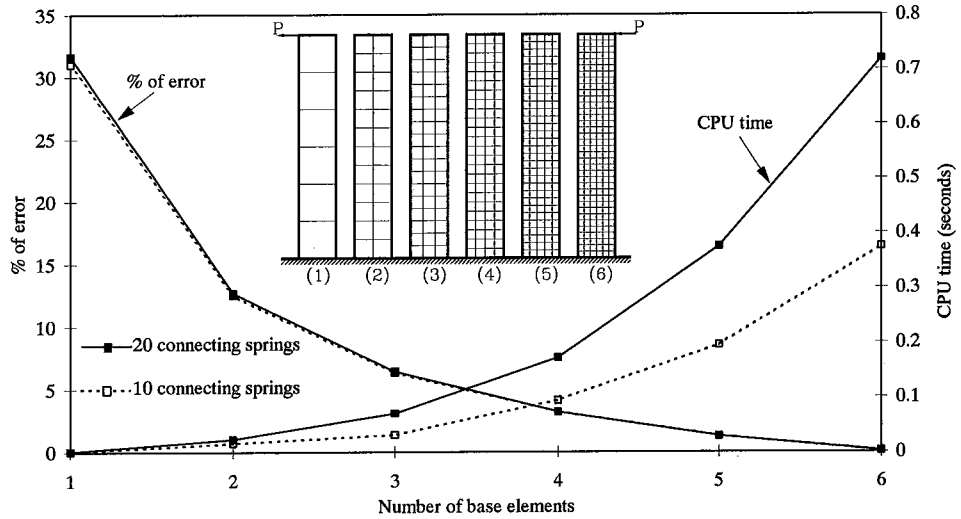


Fig. (6) Relation between the number of base elements, % of error and CPU time

## SIMULATION OF TWO-STORIED RC WALL STRUCTURE SUBJECTED TO MONOTONIC LOADING

To verify the accuracy of the model, the simulation results are compared with the experimental results of a two-storied RC wall. The shape of the wall, reinforcement and loading location are shown in Figure (7). Reference (4) gives more details on the columns, beams and wall reinforcement, or the material properties. The wall is modeled using 1,845 square elements. The number of springs between each two adjacent faces is 10. Reinforcement locations are defined by their nearest spring coordinates. For vertical reinforcement, x-coordinate is defined at the steel bar location while for horizontal reinforcement, y-coordinate is defined.

Figure (7) shows a comparison between measured and calculated load-rotation relations. First, to discuss the effects of load increment in failure analysis, three models of different load increments, calculated by dividing the estimated failure load by 50, 250 and 500, with the constant number (10) of springs were used. Next, to study the effects of the number of connecting springs between faces, additional simulations were carried out using the case of 250 load increments with 5 and 2 springs between faces and the results were compared with that with 10 springs. The failure load calculated in all cases were within the range from 64 to 70 tf while the measured one was 67 tf. The calculated failure load using the FEM was 64 tf[1]. In general, the calculated failure loads are very close to the measured ones. The results of 50, 250 and 500 increments are almost congruent till at least 90% of failure load. It should be emphasized that the CPU time of analysis of 500 increments is 10 times that of 50 increments. To avoid long CPU time, load increments can be reduced after about 90% of expected failure load. Moreover, it can be noticed easily from Figure (7) that the agreement between experimental and numerical results is fairly good for 250 increments with 10 or 5 connecting springs. Surprisingly, for the case of 250 increments with only 2 springs connecting each two adjacent faces, the results are also reliable till reaching failure of the structure. It is noted also that using few number of load increments leads to the results in slightly higher failure load (70 tf) while using a few number of connecting springs gives slightly lower one (64 tf). This means that our model gives reliable results even when using a few number of connecting springs or few number of load increments.

Although increasing the number of springs leads to increasing the CPU time required for assembling the global stiffness matrix, the time required for the solution of equations, which is dominant when the number of elements is large, does not change because the number of degrees of freedom is independent of the number of springs used. This means that we can use larger number of springs between edges without significant change of the CPU time of analysis. On the other hand, as the total number of connecting springs used is generally large, it is necessary to use automatic mesh and spring generation. Moreover, increasing the number of springs leads to increasing the computer memory capacity required.

Figure (8) shows the relation between load and the number of failed springs for each increment. Cumulative curves also show the total number of failed springs till that increment. It can be noted that although the number of increments in both cases are different, both cumulative curves close each other. This gives good indication that the solution is generally stable. Excessive cracking begins to appear when the applied load is about 28 tf. At the same load, behavior of the structure begins to be highly nonlinear.

Figure (9) shows the deformed shape during the application of load in case of 500 load increments with 10 springs. The location of cracks and crack propagation can be easily observed. The location of cracks and crack propagation are very similar to those obtained from the experiment. This means that the proposed model can be applied for fracture behavior of RC structures, such as, failure load, deformations, crack generation, crack location and crack propagation, etc.

It should be emphasized that although the shape of elements used in the analysis are squares, it does not affect the crack generation or crack propagation in the material. Diagonal cracks, as shown in Figure (9), coincide well with those obtained from the experiment. In analysis using rigid elements, like RBSM[2], shapes and distributions of elements were decided based on the assumption that cracks were generated and propagated in previously expected locations and directions.

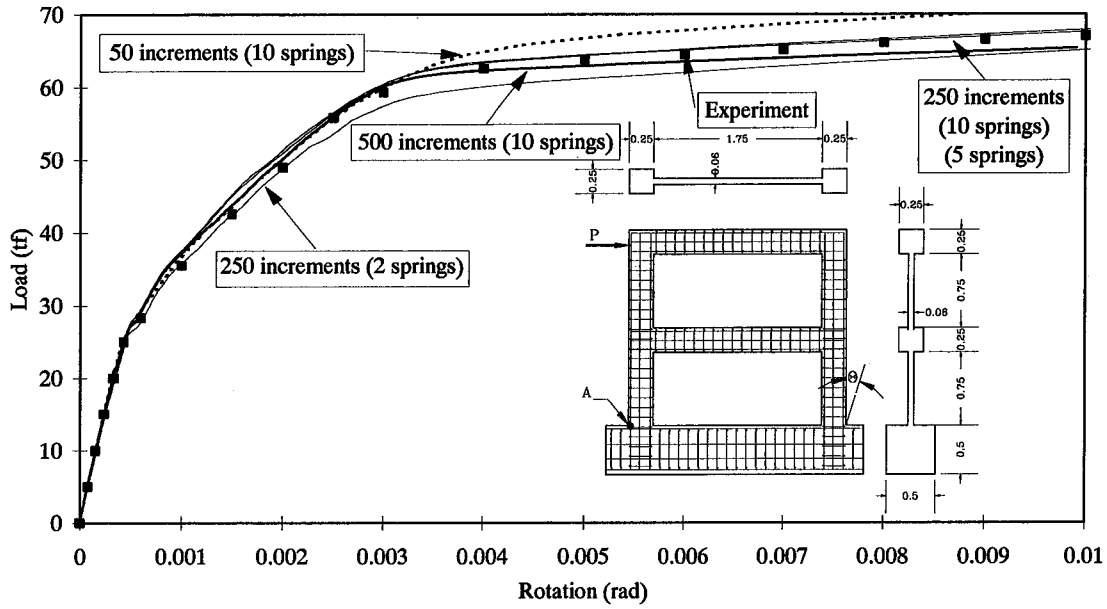


Fig. (7) Relation between load and wall rotation for 2-storied RC wall

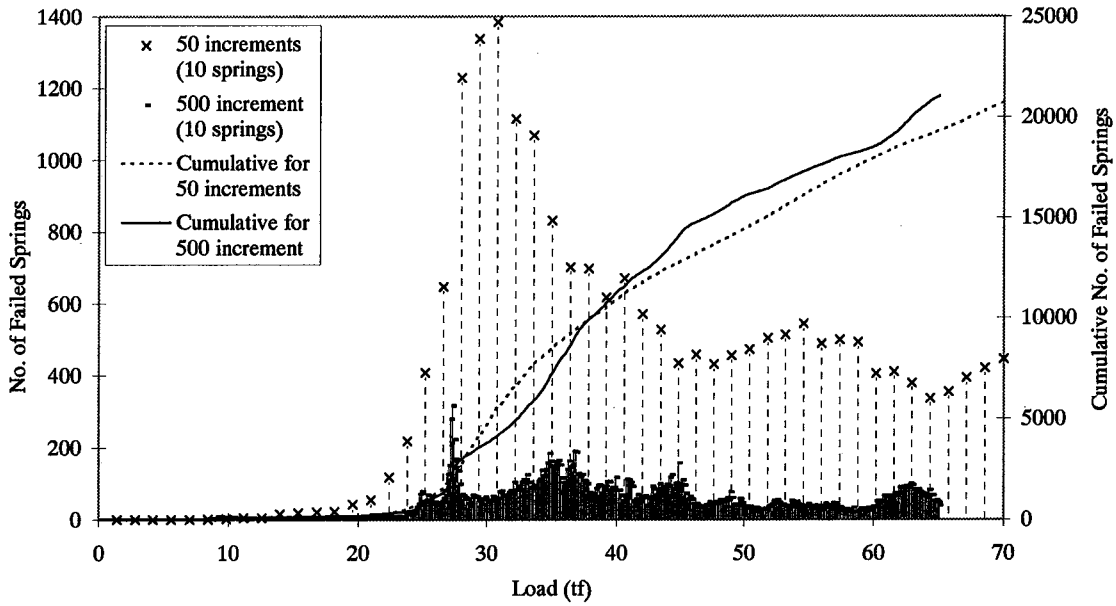


Fig. (8) Relation between load and the number of failed springs for 2-storied RC wall

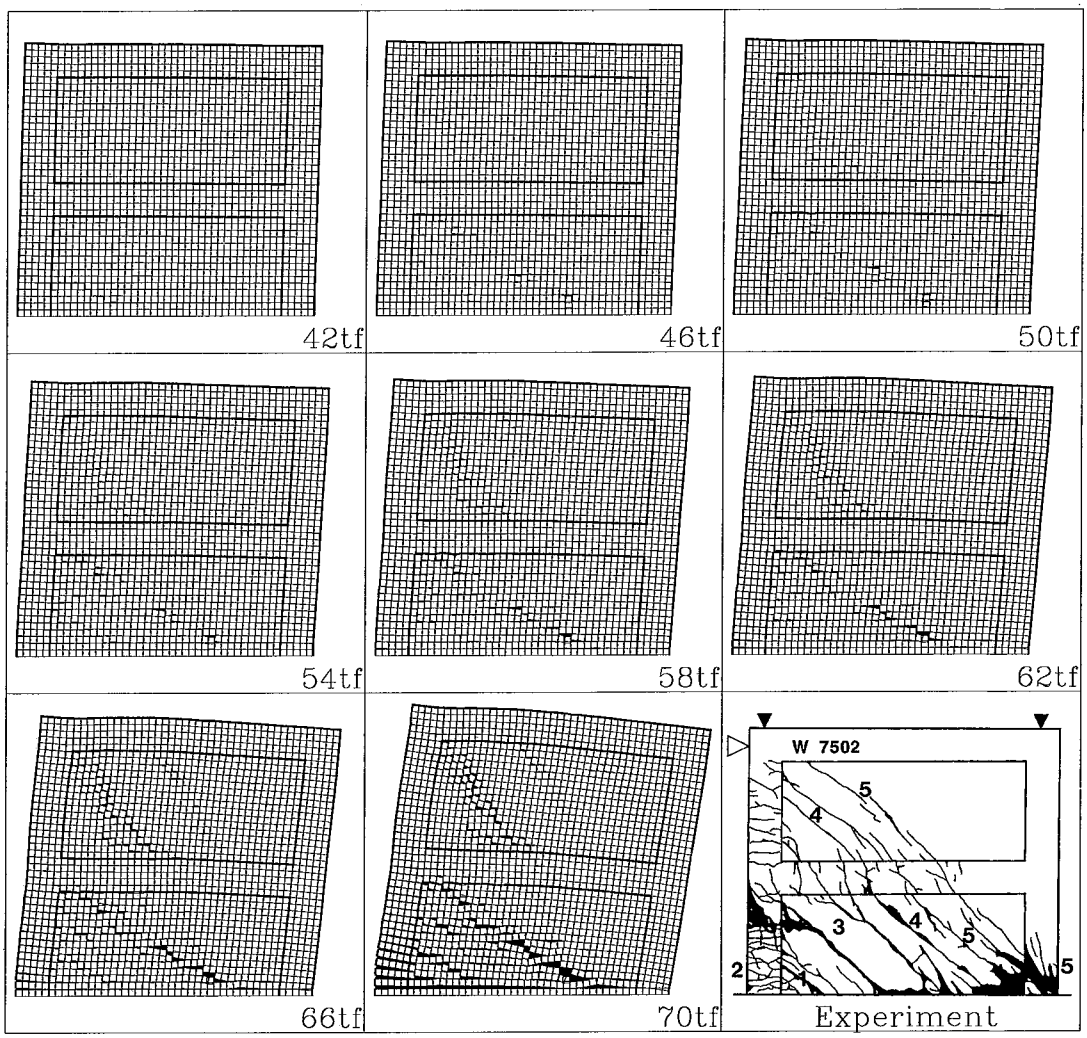


Fig. (9) Deformed shape and crack locations of the 2-storied RC wall structure
(in case of 500 increments with 10 springs between each two adjacent faces, Simulation Scale Factor=30)

## SIMULATION OF RC FRAME STRUCTURE

The third verification example is an RC frame structure. Dimensions, loading conditions and reinforcement details[6] are shown in Figure (10). This frame is modeled using 1880 elements with 10 connecting springs. The maximum load is applied in 200 increments at the shown location. It should be noted also that all reinforcement details, including stirrups location and diameters, were taken into account. Figure (10) shows also the relation between load and deformation calculated from our simulation and measured from the experiment. It can be noticed that excellent agreement between the two results has been achieved. Figure (11) shows the deformed shape and crack location at the final stage of our result and experiment. Good agreement between the measured and calculated crack locations, crack inclination and crack length can also be obtained. In both experiment and numerical simulation, failure occurs near the base and at connections.

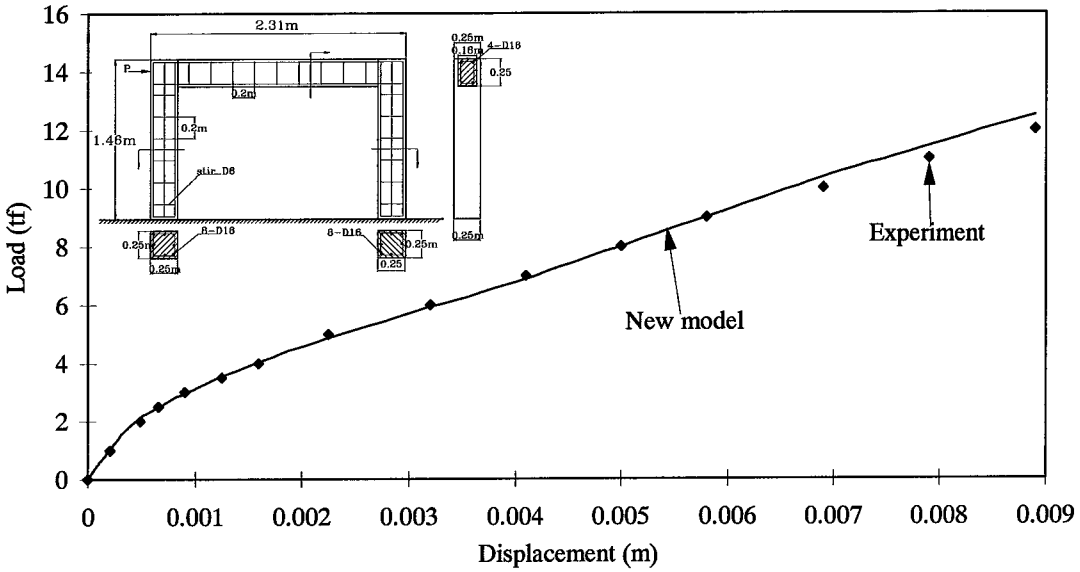


Fig. (10) Relation between load and maximum displacement at the loading point of RC frame

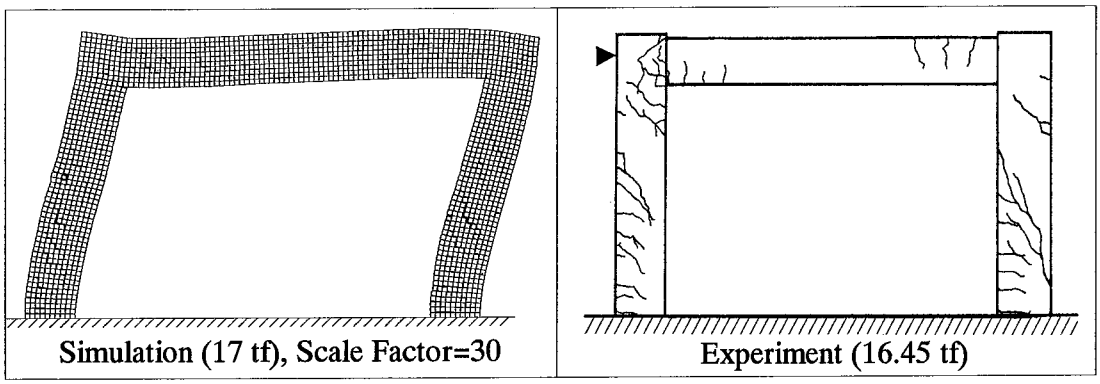


Fig. (11) Deformed shape of RC frame

## SIMULATION OF RC DEEP BEAMS WITHOUT SHEAR REINFORCEMENT BARS

In this section, simulation results of two deep beams[7] which do not have shear reinforcement in the shear zone are introduced. This type of analysis is generally difficult because of excessive cracking which occurs during loading. The results obtained through our model are compared with the experimental results and FEM results as shown in Figures (12) and (13). The shape, loading conditions, reinforcement and deformed shape are also shown in these figures. In general, the results of the proposed model are more accurate than those obtained with the FEM. The accuracy of the FEM decreases and finally becomes impossible to apply the FEM when the ratio between shear zone length and the total beam length increases. The reason is simply because no reinforcement is used in the shear zone and hence, the sensitivity of the concrete to cracking increases. This effect can not be accurately followed using the FEM.

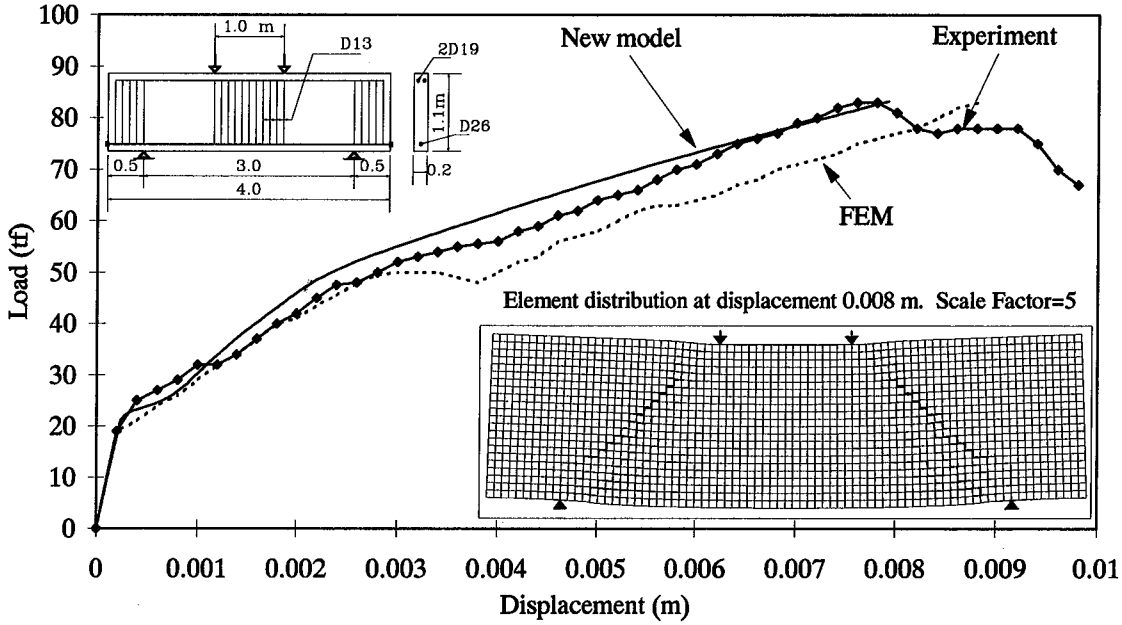


Fig. (12) Shape and results of a two point loading deep beam without shear reinforcement

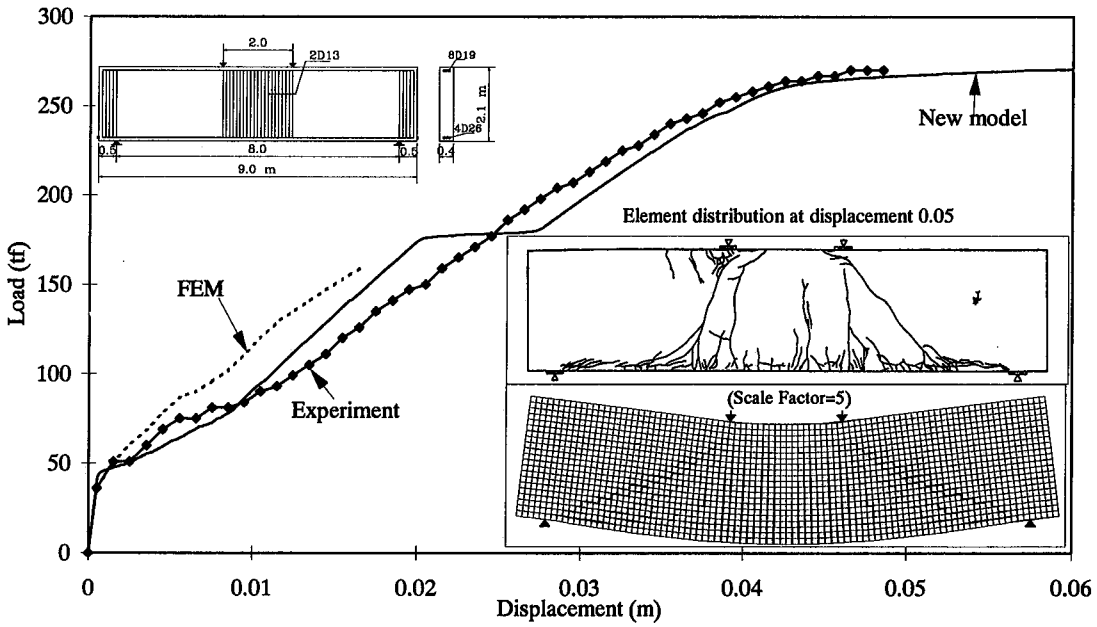


Fig. (13) Shape and results of a two point loading deep beam without shear reinforcement

## MATERIAL MODELING FOR CYCLIC LOADING

For concrete springs subjected to cyclic loading, Maekawa's compression model[8] shown in Figure 14(a) is adopted to simulate cyclic stress-strain relation. On the other hand, for reinforcement, the steel model shown in Figure 14(b) is used[9]. The main advantage of these models are that they incorporate only one equation for the simulation of behavior in loading, unloading, reloading and post peak behaviors. Stress-strain relation for concrete springs subjected to tension is assumed linear till reaching the cracking point and then the stiffness is assumed zero.

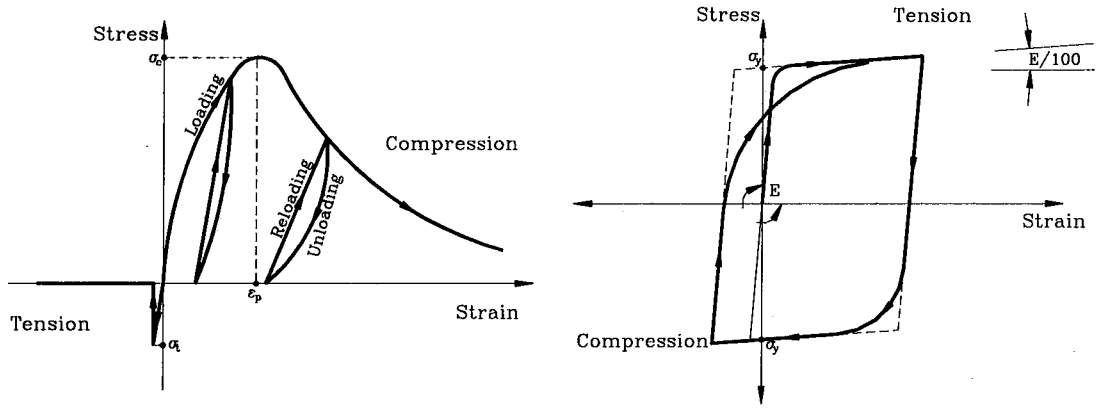


(a) Concrete (b) Steel

Fig. (14) Material models for steel and concrete

## SIMULATION OF TWO-STORIED RC WALL STRUCTURE SUBJECTED TO CYCLIC LOADING

To verify the accuracy of the model under cyclic loading, the simulation results are compared with the experimental results of the two-storied RC wall structure in cyclic loading conditions. The applied cyclic load is shown in Figure (15). The wall shape, reinforcement and loading point were shown in Figure (7). Figure (16) shows the number of failed springs during loading. It is obvious that this number always has a peak when the applied load is maximum and then decreases in the unloading stage. Figure (17) shows the relation between load and angle of rotation ($\theta$) during the loading. It seems from the relation shown in Figure (17) that the value of plastic strain and unloading behavior are not so accurate because of element dislocations during loading process. This leads to incomplete cracking closure and hence the unloading stiffness becomes less than the measured one. Figure (18) shows the stress-strain relation for steel bars located at point "A". It can be noticed that the value of tensile strain is larger than that of compressive strains. The reason is crack closure in compression. It should be emphasized that it is very easy to follow all reinforcement details and any stress-strain relation at any point for the studied structure. With the FEM, it is practically impossible to follow all reinforcement details in the analysis. Figure (19) shows the deformed shape and crack locations in the specimen. It is clear that the crack locations are very near to those from the experiment. The generated cracks open and close in such a way which is similar to what happens in the experiment. These cracks are generated without use of any special techniques, such as joint elements in FEM, and without assuming the crack location and direction of propagation before the analysis.

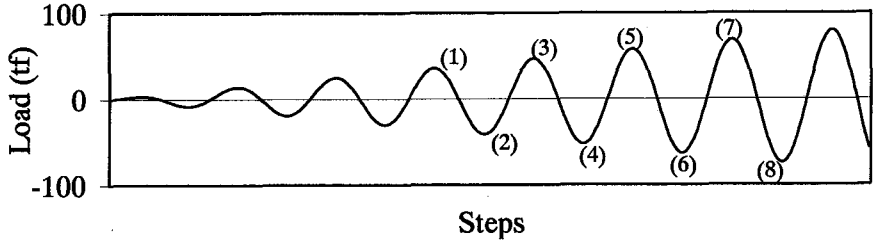


Fig. (15) Load pattern

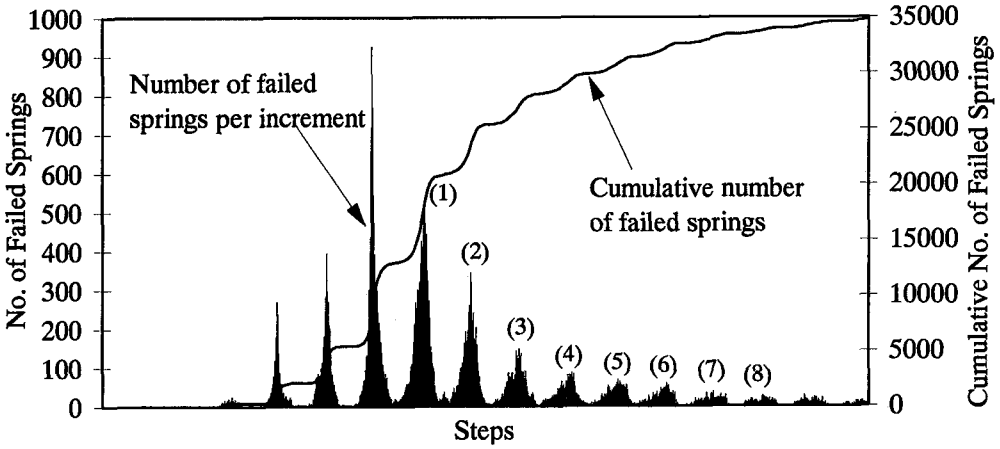


Fig. (16) Number of failed springs for each step

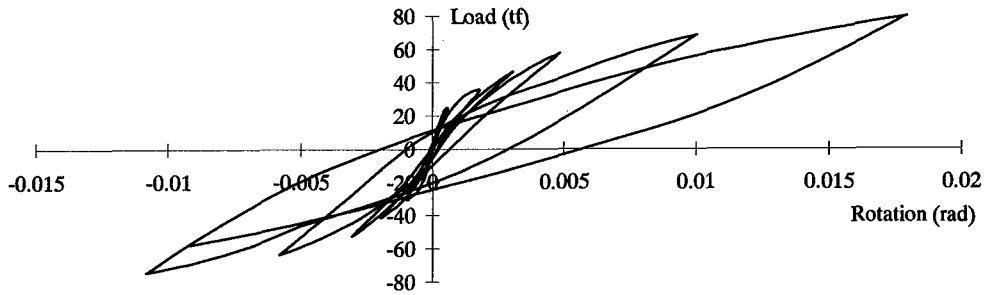


Fig. (17) Relation between load and rotation (θ)

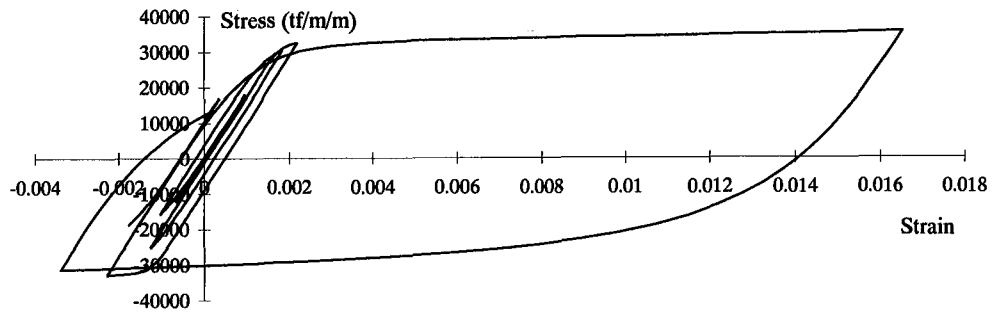


Fig. (18) Stress-strain relation at point "A" at the base of left column

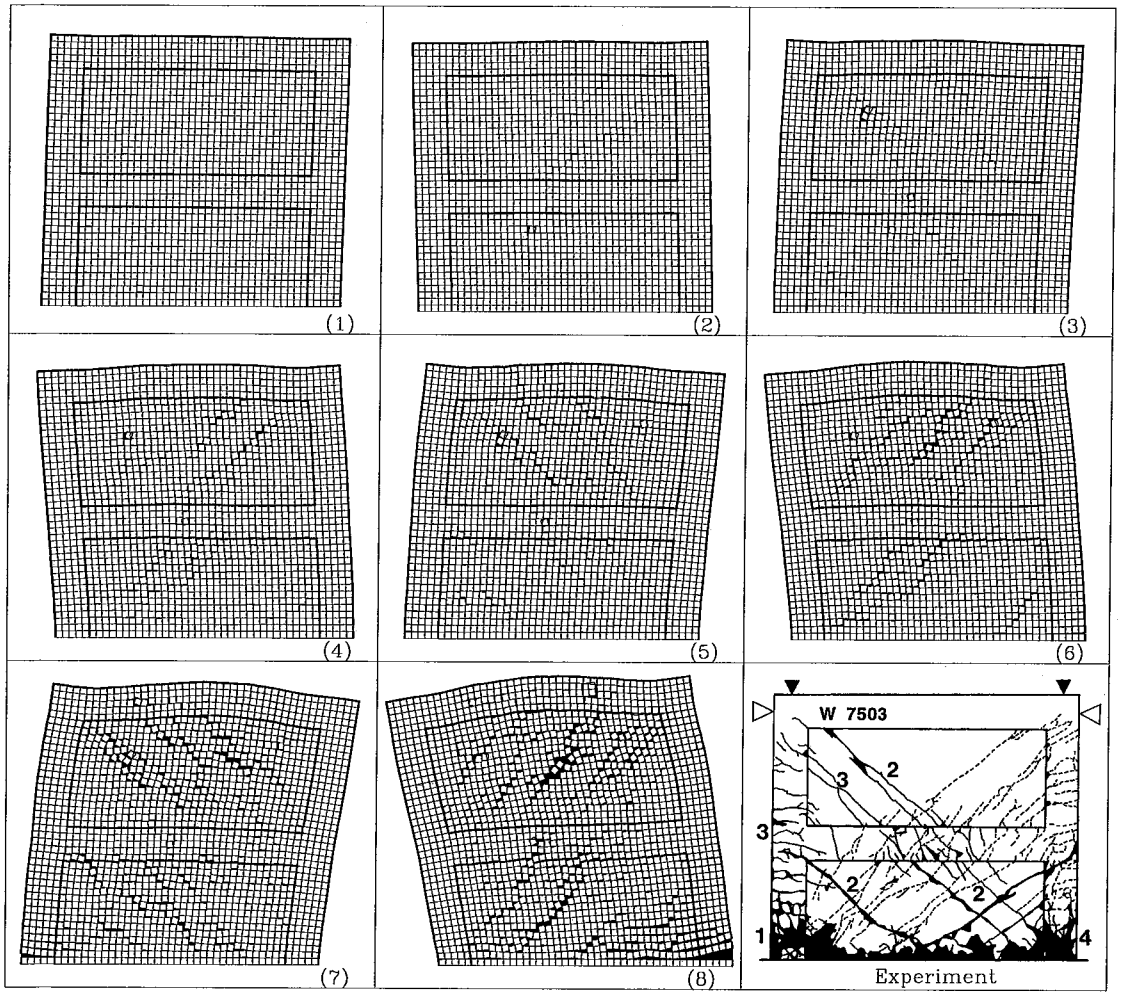


Fig. (19) Deformed shape and crack location at different loading stages (Simulation Scale Factor=30)

## CONCLUSIONS

Through numerical simulations of reinforced concrete structures, it is confirmed that the new proposed model is capable of simulating the fracture behavior of concrete structures. The results of load and displacements in monotonic loading almost coincide with the experimental results by at least 95% accuracy. The expected failure mode is also very close to the measured one. Through this new model, stresses, strains, deformations, crack initiation and propagation of cracks can be calculated with high accuracy and relatively simple techniques. In addition, all reinforcement details, such as bar location and shear reinforcement details, can be taken into account without any additional complications to the analysis. Also, it is very easy to follow the mechanical behavior of steel and concrete at any point. Although the shape of the element used was square, it did not affect the crack propagation in the material. Even though the formulations used for the material properties were relatively simple, the results obtained are better or of the same accuracy of the FE analysis. This method does not require any complicated models for the representation of cracking or special elements, such as joint elements, to follow the crack propagation, the results obtained by the proposed method in monotonic loading condition agree well with experimental results. However, for cyclic

loading, further research may improve the accuracy of unloading behavior. This model can be easily combined with the EDEM to simulate the total behavior of structure till complete failure. The proposed model is expected to give high accuracy to wide applications where FEM does not give reliable accuracy.

## REFERENCES


1. Okamura H. and Maekawa K.: Nonlinear analysis and constitutive models of reinforced concrete, Gihodo Co. Ltd., Tokyo, 1991.
2. Kawai T.: Some considerations on the finite element method, Int. J. for Numerical Methods in Engineering, Vol. 16, pp. 81-120, 1980.
3. Meguro K. and Hakuno M.: Fracture analyses of concrete structures by the modified distinct element method, Structural Eng./Earthquake Eng., Japan Society of Civil Engineers, Vol. 6., No. 2, pp. 283s-294s, October, 1989.
4. Hajime Ono et al.: Study on seismic capacity of reinforced concrete shear wall, Part 7, Relation between load history and horizontal reinforcement, Proc. of annual conference of Architectural Institute of Japan (AIJ), pp. 1601-1602, 1976. (in Japanese)
5. Niwa J., Maekawa K. and Okamura H.: Nonlinear finite element analysis of deep beams, 10th annual lecture on "FEM Analysis of Reinforced Concrete Structures", Civil Engineering Department, The University of Tokyo, 1995.
6. Muto K.: Strength and deformations of structures, Maruzen Co. Ltd., 1965. (in Japanese)
7. Railroad Research Institute and Research Institute of Tekken Co. Ltd.: Study on shear capacity of RC members based on fracture mechanics, Internal report, 1997. (in Japanese)
8. Okamura H., Maekawa K. and Izumo J.: Reinforced concrete plate element subjected to cyclic loading, 10th annual lecture on "FEM Analysis of Reinforced Concrete Structures", Civil Engineering Department, The University of Tokyo, 1995.
9. Ristic D., Yamada Y., and Iemura H.: Stress-strain based modeling of hystertic structures under earthquake induced bending and varying axial loads, Research report, No. 86-ST-01, School of Civil Engineering, Kyoto University, March, 1986.